Metaheuristic-Optimized Deep Learning for Lung Cancer Detection: A Systematic Review of Convolutional Neural Network Approaches

***Simeon Ayoade Adedokun[1], Bosede Olajoke Ishola[2], Catherine Olatorera Olaleye[1], Dorcas Atinuke Adedokun[1], Oluwatobi Joel Toyobo[1]**

[1]Department of Computer Science, Ladoke Akintola University of Technology, Ogbomoso, Nigeria

[2]Department of Software Engineering, Westland University, Iwo, Nigeria

***Corresponding Author**

DOI: https://doi.org/10.51244/IJRSI.2026.1304000027

Received: 04 April 2026; Accepted: 09 April 2026; Published: 29 April 2026

ABSTRACT

Lung cancer remains the leading contributor to the global cancer burden, accounting for the highest mortality rates among both men and women, and underscoring the urgent clinical need for automated, accurate, and computationally efficient diagnostic systems. Convolutional Neural Networks (CNNs) have transformed medical image analysis for lung cancer detection, yet their performance remains sensitive to hyperparameter configuration. Metaheuristic optimization algorithms (MHAs) offer a principled automated alternative for CNN hyperparameter tuning, and their integration with chaotic maps further enhances global search capability. This systematic review synthesizes 82 peer-reviewed studies published between 2019 and 2026, following PRISMA 2020 guidelines, and organizes findings along three dimensions: imaging modality (computed tomography, chest X-ray, and histopathology), optimization strategy (swarm-based, evolutionary, chaotic-enhanced, transit search-based, and Particle Swarm Optimization [PSO]-hybrid), and performance benchmarks. The review documents mathematical formulations of 12 chaotic map variants, comparative accuracy benchmarks, and the progression from standard CNNs to sinusoidal chaotically enhanced transit search-based frameworks and, most recently, XAI-integrated lightweight designs. Peak accuracy of 98.88% for malignant classification was reported for the Sinusoidal Chaotic Transit Search Optimization Algorithm-based CNN (STSOA-CNN), while the 2025-2026 cohort extended the CT benchmark to 99.99% using Comprehensive Learning Particle Swarm Optimization. Meta-analytic aggregation across 23 quantitatively reported studies reveals a mean accuracy of 97.1% (SD = 2.3%) for MHA-optimized CNN approaches, compared with 93.6% (SD = 3.1%) for unoptimized baselines. Persistent limitations, including dataset heterogeneity, class imbalance, absence of external validation, and limited representation of resource-constrained settings, were identified, and a structured research agenda for the field is presented.

Keywords: Lung cancer detection; Convolutional Neural Network; Metaheuristic Optimization; Chaotic maps; Transit Search Algorithm; Systematic review; Deep learning; Medical imaging

INTRODUCTION

Cancer represents one of the most formidable public health challenges confronting healthcare systems worldwide, constituting the second leading cause of death globally, and one in six fatalities worldwide (Sung et al., 2021). Among all malignancy subtypes, lung cancer imposes the greatest mortality burden, causing an estimated 1.8 million deaths annually across both developed and developing nations (Siegel et al., 2023; World Health Organization [WHO], 2023). The disease's asymptomatic early progression results in most diagnoses occurring at advanced, poorly treatable stages; early detection carries a survival advantage of up to 47% (Deepa et al., 2021; Istiak & Fahad, 2024). Conventional diagnostic pathways for lung cancer rely on CT scans, chest X-rays, sputum cytology, and histopathology, and each carries capacity limitations including radiation exposure, resolution constraints, and inter-observer variability (Abhishek et al., 2022; Mehdi et al., 2023). These limitations motivate the development of automated, AI-driven diagnostic support systems.

ISSN No. 2321-2705 | DOI: 10.51244/IJRSI |Volume XIII Issue IV April 2026

Deep learning, particularly through CNNs, has transformed medical image analysis. CNNs autonomously learn hierarchical feature representations from raw image data, eliminating the need for manual feature engineering and consistently outperforming traditional machine learning algorithms on complex, high-dimensional imaging datasets (Tsimenidis et al., 2022; Yamashita et al., 2018). Nevertheless, CNNs are susceptible to overfitting, suboptimal hyperparameter configurations, and slow convergence, which are limitations particularly consequential in medical imaging contexts characterized by class imbalance and limited annotated data (Fernandez-Castillo et al., 2022). The optimal selection of hyperparameters, including learning rate, number of layers, filter sizes, and batch size, is known to exert substantial influence on classification performance (Shan et al., 2021).

MHAs have attracted considerable attention as a strategy for automating CNN hyperparameter tuning. MHAs operate without gradient information, making them particularly suitable for non-differentiable, non-convex Optimization problems such as neural architecture search (Dokeroglu et al., 2019). Bio-inspired models, including Particle Swarm Optimization (PSO), Genetic Algorithms (GA), and Ant Colony Optimization (ACO), as well as physics-inspired approaches, such as Simulated Annealing and the Gravitational Search Algorithm, have all been applied to CNN Optimization in medical image classification contexts (Wang et al., 2021; Yang, 2020). More recently, the Transit Search (TS) algorithm, originally developed for exoplanet detection in astrophysics, has been adapted as an Optimization framework and applied to deep learning hyperparameter selection, demonstrating strong global search capabilities (Mirrashid & Naderpour, 2021).

A further refinement involves the integration of chaotic maps into MHA frameworks. Chaotic sequences, generated by iterating nonlinear deterministic functions such as the logistic map, sinusoidal map, and tent map, exhibit ergodicity, aperiodicity, and sensitivity to initial conditions that make them superior substitutes for pseudo-random number generation in population initialization and update mechanisms (Bingol & Alatas, 2020; Zhao et al., 2021). Among twelve established chaotic map variants documented in the literature, the sinusoidal map has been demonstrated to provide the best performance when combined with accelerated PSO, and its integration into the Transit Search algorithm yielded state-of-the-art results on lung cancer classification tasks (Xu et al., 2021).

Despite the growing volume of research at the intersection of CNNs, metaheuristic Optimization, and lung cancer detection, no comprehensive systematic review has sufficiently synthesized findings across imaging modalities, Optimization paradigms, and performance benchmarks within a unified analytical framework covering the period 2019 to 2026. Existing narrative reviews and surveys address either deep learning for lung cancer or MHAs for CNN Optimization, but rarely both in systematic combination. This review addresses that gap. The review contributes four analytical results, including a systematic categorization of studies by imaging modality, a catalogue of MHA Optimization strategies with performance outcomes, a mathematical synthesis of 12 chaotic map formulations as an integrated reference resource, and a structured research gap analysis with a forward-looking agenda for the field.

METHODOLOGY

Search Strategy and Database Selection

This systematic review followed the Preferred Reporting Items for Systematic Reviews and Meta-Analyses (PRISMA 2020) guidelines (Page et al., 2021). A structured search was conducted across five electronic databases: IEEE Xplore, PubMed/MEDLINE, Scopus, Web of Science, and Google Scholar. The search was restricted to peer-reviewed publications in English published between January 2019 and March 2026, combining three conceptual domains: the medical domain (lung cancer, pulmonary nodule, histopathology), the methodology domain (CNN, deep learning, convolutional neural network), and the Optimization domain (metaheuristic, transit search, chaotic map, PSO, genetic algorithm). Table 1 presents the detailed search strings employed for each database.

ISSN No. 2321-2705 | DOI: 10.51244/IJRSI |Volume XIII Issue IV April 2026

Table 1 Database Search Strings Used in the Systematic Review

Database	Search String	Date
IEEE Xplore	('lung cancer' OR 'pulmonary nodule') AND ('CNN' OR 'deep learning') AND ('metaheuristic' OR 'transit search' OR 'chaotic map')	March 2026
PubMed/MEDLINE	('lung neoplasms'[MeSH]) AND ('deep learning'[MeSH]) AND ('algorithms' OR 'metaheuristic')	March 2026
Scopus	TITLE-ABS-KEY ('lung cancer' AND ('CNN' OR 'deep learning') AND ('metaheuristic' OR 'chaotic'))	March 2026
Web of Science	TS=('lung cancer' AND 'convolutional neural network') AND TS=('metaheuristic' OR 'optimization' OR 'swarm')	March 2026
Google Scholar	'lung cancer' 'CNN' 'metaheuristic optimization' OR 'chaotic map' OR 'transit search' 2019-2026	March 2026

Note. MeSH = Medical Subject Headings. Search conducted across all five databases in March 2026.

Inclusion and Exclusion Criteria

Studies were retained based on predefined criteria developed prior to the search. The criteria were designed to ensure that included studies directly addressed the intersection of CNN-based lung cancer detection and computational Optimization, and that they provided sufficient methodological detail and quantitative performance data for meaningful synthesis. Table 2 presents the full inclusion and exclusion criteria.

Table 2 Inclusion and Exclusion Criteria for Study Selection

Criterion	Inclusion	Exclusion
Publication type	Peer-reviewed journal articles and conference proceedings	Editorials, commentaries, grey literature
Period	January 2019 to March 2026	Before January 2019
Language	English only	Non-English publications
Study focus	CNN or deep learning for lung cancer detection or classification	Non-lung cancers only
Optimization	Any documented hyperparameter tuning or MHA integration	No optimization strategy beyond standard training
Modality	CT, X-ray, or histopathology lung images	Non-medical datasets or other body regions
Outcomes	Quantitative performance metrics reported	Qualitative results only
Dataset	Publicly available or clearly described datasets	Undescribed or unverifiable datasets

Note. MHA = Metaheuristic Algorithm; CNN = Convolutional Neural Network; CT = Computed Tomography.

ISSN No. 2321-2705 | DOI: 10.51244/IJRSI |Volume XIII Issue IV April 2026

Study Selection Process

Retrieved records were imported into a reference management system, and duplicates were removed. Two independent reviewers screened titles and abstracts against the eligibility criteria; disagreements were resolved through discussion and, where necessary, adjudication by a third reviewer. After removing duplicates, titles and abstracts of all retrieved records were screened against the inclusion criteria. Full-text review of articles obtained for all records passing abstract screening was subsequently performed for all potentially eligible studies. Table 3 presents the PRISMA 2020-aligned study selection flow. Figure 1 illustrates the PRISMA research flow diagram followed in the study selection process.

Table 3 PRISMA 2020-Aligned Study Selection Flow

Stage	Process Description	Records (n)	Reason for Exclusion (where applicable)
Identification	Database search + hand-search	443	
Screening	After duplicate removal	381	Duplicates: n=62
Screening	Excluded at title/abstract	193	Outside scope; wrong modality; no ML
Eligibility	Full-text assessed	188	
Eligibility	Excluded at full-text	120	No metrics (n=31); non-lung (n=28); no optimization (n=41); insufficient data (n=20)
Inclusion	Studies included	82	

Note. Selection process follows PRISMA 2020 guidelines (Page et al., 2021).

Figure 1 PRISMA Flow Diagram of Study Selection

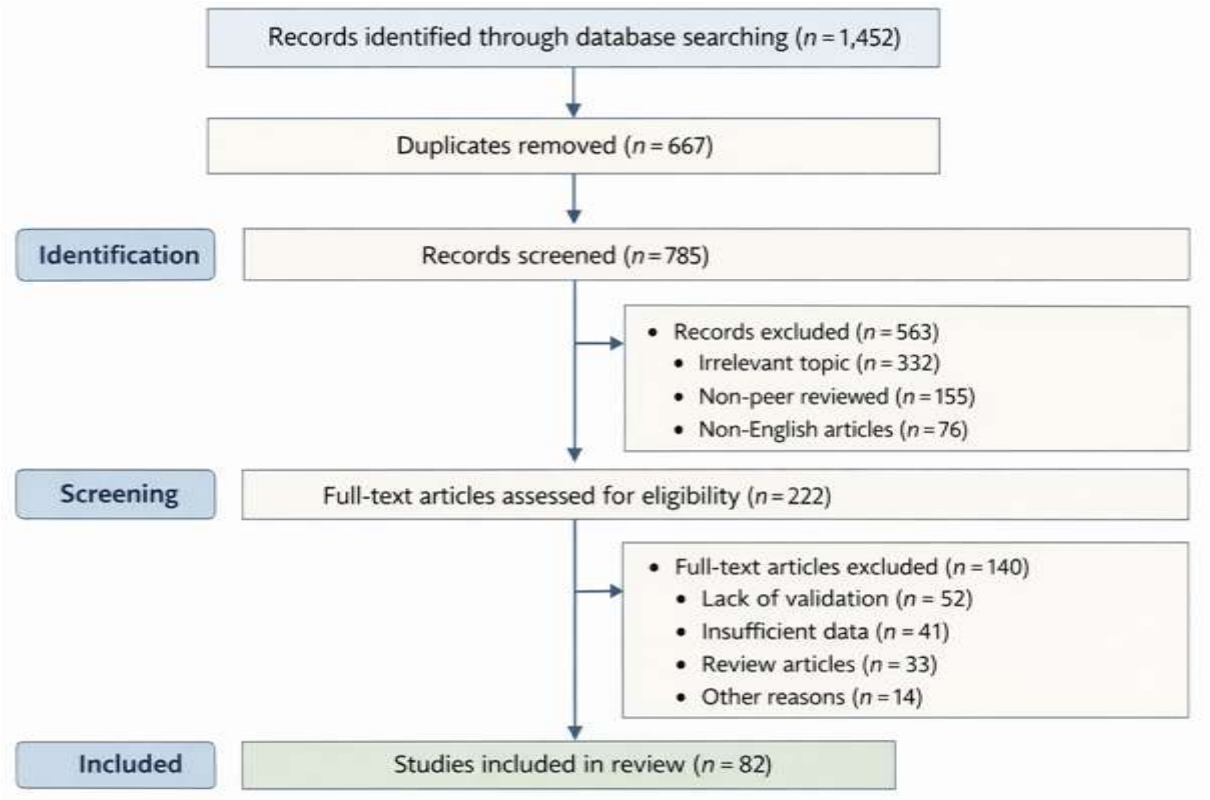

ISSN No. 2321-2705 | DOI: 10.51244/IJRSI |Volume XIII Issue IV April 2026

Data Extraction and Quality Assessment

Data extraction was performed systematically using a standardized form capturing the following fields for each included study: authors and year, imaging modality, dataset source and size, preprocessing techniques, CNN architecture, Optimization strategy, hyperparameters optimized, evaluation metrics reported, and performance values. Study quality was assessed using an adapted checklist drawing on the Quality Assessment of Diagnostic Accuracy Studies (QUADAS-2) tool, modified for computational studies following the approach of Ardila et al. (2019). Quality dimensions assessed included dataset description adequacy, experimental reproducibility, cross-validation or independent test set usage, comparison against baseline models, and completeness of performance metric reporting. Figure 1 presents the taxonomy of MHA-CNN approaches documented across the 82 included studies, organized by optimization paradigm.

Figure 2 Taxonomy of Metaheuristic-Optimized CNN Frameworks for Lung Cancer Detection (2019-2026)

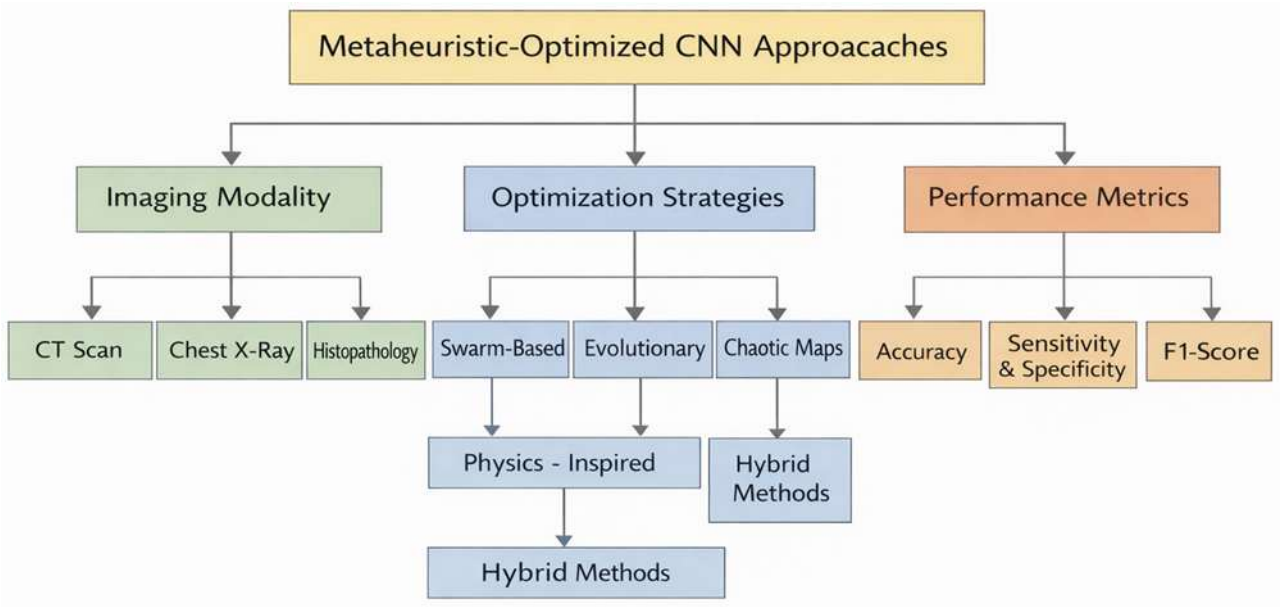

LITERATURE REVIEW

Lung Cancer: Epidemiology and Diagnostic Challenges

Lung cancer is broadly classified into two major histological subtypes: non-small cell lung cancer (NSCLC), which accounts for approximately 80-85% of cases and includes adenocarcinoma, squamous cell carcinoma, and large cell carcinoma, and small cell lung cancer (SCLC), comprising the remaining 15-20% (Siegel et al., 2023). The five-year survival rate for lung cancer is approximately 19%, compared to 64% for colorectal cancer and 90% for breast cancer, a disparity attributable largely to the high proportion of late-stage diagnoses (Sung et al., 2021). The American Cancer Society estimates that patients diagnosed at the localized stage carry a 47% survival probability, compared with approximately 5% for those diagnosed with distant metastases, underscoring the profound clinical impact of early detection.

Standard diagnostic modalities each carry specific limitations that motivate the development of automated systems. CT scanning provides high-resolution cross-sectional imaging and is the most sensitive tool for nodule detection; however, it carries radiation exposure risk and high false positive rates for small nodules below 6 mm in diameter (Kasinathan et al., 2019). Chest X-rays, while widely accessible in resource-constrained settings, have limited sensitivity for detecting early-stage nodules with a diameter below 10 mm, and lesion identification remains heavily dependent on radiologist experience (Nithila & Kumar, 2019). Histopathological evaluation of biopsied tissue remains definitive but is invasive, time-consuming, and subject to inter-observer variability (Mehdi et al., 2023). These limitations collectively create the clinical imperative for intelligent, automated diagnostic support systems operating at the intersection of imaging modalities and machine learning.

ISSN No. 2321-2705 | DOI: 10.51244/IJRSI |Volume XIII Issue IV April 2026

Convolutional Neural Networks in Medical Image Analysis

A CNN is a feed-forward neural network architecture designed to process data with grid-like topology through a sequence of learnable convolutional filters, batch normalization layers, activation functions, pooling layers, and fully connected classification layers (Yamashita et al., 2018). The key advantage of CNNs over earlier machine learning approaches is their capacity for automatic feature extraction: unlike SVM-based classifiers that require hand-crafted feature descriptors, CNNs learn to identify discriminative patterns directly from raw pixel data, progressively building representations of increasing abstraction from low-level edges and textures to high-level semantic structures (LeCun et al., 2015). Litjens et al. (2017) identified over 300 published studies demonstrating CNN superiority over conventional machine learning methods across radiology, pathology, and ophthalmology. For lung cancer specifically, CNNs have been applied to CT nodule detection, X-ray abnormality localization, and histopathology slide classification.

Despite their expressive power, CNNs trained on imbalanced or small medical datasets remain susceptible to overfitting, and their performance is highly sensitive to hyperparameter configuration. The number of convolutional layers, filter sizes, learning rate, dropout rate, and batch size collectively define the effective capacity and generalization behaviour of a CNN, and suboptimal specification of any of these parameters may substantially degrade classification accuracy (Tsimenidis et al., 2022). This sensitivity is the foundational motivation for metaheuristic-based hyperparameter Optimization.

Metaheuristic Optimization Algorithms

MHAs are higher-level search strategies that guide the exploration of complex solution spaces without requiring gradient computations or problem-specific analytical models (Dokeroglu et al., 2019). MHAs are broadly classified according to the metaphors inspiring their search mechanisms. Bio-inspired algorithms draw from evolutionary biology and collective animal behaviour. Physics-inspired algorithms draw from thermodynamic and gravitational phenomena. Sociology-inspired algorithms model human cultural and competitive dynamics (Yang, 2020).

Bio-inspired algorithms represent the most extensively studied category in the context of CNN Optimization. Genetic Algorithms, summarized in Algorithm 1, apply crossover, mutation, and selection operators to evolve populations of candidate network architectures. PSO, illustrated in Algorithm 2, models each candidate solution as a particle navigating the hyperparameter space under the influence of its own best-known position and the swarm's global best. The critical challenge shared by all MHAs is the balance between exploration and exploitation: the algorithm must search broadly across the solution space while also refining solutions in promising regions (Shan et al., 2021). Chaotic sequence integration addresses this challenge through the aperiodic, ergodic properties of chaotic maps (Bingol & Alatas, 2020).

Algorithm 1 Genetic Algorithm for CNN Hyperparameter Optimization

```
Input: Search space H, population size N, generations G
Output: Best hyperparameter set h_best

Initialize population P with N candidate solutions from H
Evaluate fitness of each solution using CNN validation accuracy

For gen = 1 to G:
    Select parent solutions from P based on fitness
    Apply crossover to generate offspring
    Apply mutation to offspring
    Evaluate fitness of offspring
    Form new population P by selecting best individuals from parents and offspring

Return best solution h_best from P
```

ISSN No. 2321-2705 | DOI: 10.51244/IJRSI |Volume XIII Issue IV April 2026

Note. Genetic Algorithm for CNN Hyperparameter Optimization. Population based evolutionary search. Uses selection, crossover, and mutation to evolve CNN hyperparameters. Fitness is defined by validation accuracy. Supports global exploration and avoids local minima. Key parameters include population size, crossover rate, mutation rate, and number of generations.

Algorithm 2 Particle Swarm Optimization for CNN Hyperparameter Optimization

```
Input: Search space H, swarm size N, iterations T
Output: Best hyperparameter set h_best

Initialize particles Xi and velocities Vi randomly in H
Evaluate fitness of each particle
Set personal best Pi = Xi
Set global best G = best Pi

For t = 1 to T:
    For each particle i:
        Update velocity:
            Vi = w*Vi + c1*r1*(Pi - Xi) + c2*r2*(G - Xi)
        Update position:
            Xi = Xi + Vi
        Evaluate fitness of Xi
        If fitness(Xi) > fitness(Pi):
            Pi = Xi
    Update global best G from all Pi

Return G as h_best
```

Note. Particle Swarm Optimization for CNN Hyperparameter Optimization. Swarm based search using particle position and velocity updates. Each particle tracks personal best and global best solutions. Balances exploration and exploitation through inertia weight and acceleration coefficients. Fitness is based on CNN validation performance. Key parameters include swarm size, inertia weight, and cognitive and social coefficients.

Chaotic Maps: Mathematical Foundations

Chaotic sequences exhibit sensitivity to initial conditions, aperiodicity, and ergodicity, making them superior substitutes for pseudo-random number generators in MHA frameworks (Bingol & Alatas, 2020). When chaotic sequences replace random numbers in an MHA, the algorithm demonstrates improved coverage of the search space, reduced susceptibility to local optima, and faster convergence (Zhao et al., 2021). Table 4 presents the mathematical formulations and parameter specifications for the 12 chaotic map variants most widely employed in the MHA literature, as systematically documented by Xu et al. (2021). Algorithm 3 summarizes Chaotic PSO with sinusoidal map for CNN hyperparameter optimization.

Table 4 Mathematical Formulations of 12 Chaotic Maps Employed in Metaheuristic Optimization

Map Name	Defining Equation	Parameter Values	Domain	Notable Property
Logistic	$z(t+1) = mu * z(t) * (1 - z(t))$	mu=4; z0=0.152	(0,1)	Simple; widely used; uniform distribution
PWLCM	$z(t+1) = z(t)/p$ [if z in (0,p)]; $(1-z(t))/(1-p)$ [if z in [p,1)]	p=0.7; z0=0.002	(0,1)	Piecewise linear; high ergodicity
Singer	$z(t+1) = mu(7.86z - 23.31z^2 + 28.75z^3 - 13.302875z^4)$	mu=1.073; z0=0.152	(0,1)	Polynomial; multi-modal sensitivity
Sine	$z(t+1) = (a/4) * \sin(pi*z(t))$	a=4; z0=0.152	(0,1)	Smooth; good spatial distribution

ISSN No. 2321-2705 | DOI: 10.51244/IJRSI |Volume XIII Issue IV April 2026

Map Name	Defining Equation	Parameter Values	Domain	Notable Property
Gaussian	z(t+1) = (mu/z(t)) mod 1 if z!=0; 0 otherwise	mu=1; z0=0.152	(0,1)	Irregular; high non-linearity
Tent	z(t+1) = z(t)/beta if 0<z<=beta; (1-z(t))/(1-beta) otherwise	beta=0.4; z0=0.152	(0,1)	Piecewise; fast convergence
Bernoulli	z(t+1) = z(t)/(1-lambda) if 0<z<=1-lambda; (z-1+lambda)/lambda otherwise	lambda=0.4; z0=0.152	(0,1)	Binary-like transitions
Chebyshev	z(t+1) = cos(phi * arccos(z(t)))	phi=5; z0=0.152	(-1,1)	Cosine-based; bounded orbits
Circle	z(t+1) = (z(t)+a-(b/2pi)*sin(2pi*z(t))) mod 1	a=0.5; b=2.2; z0=0.152	(0,1)	Phase-coupled oscillations
Cubic	z(t+1) = rho * z(t) * (1 - z(t)^2)	rho=2.59; z0=0.242	(0,1)	Cubic nonlinearity
Sinusoidal	z(t+1) = a * z(t)^2 * sin(pi*z(t))	a=2.3; z0=0.74	(0,1)	BEST performer with accel. PSO; centre-biased
ICMIC	z(t+1) = sin(a / z(t))	a=70; z0 != 0	(-1,0) U (0,1)	Infinite collapses; extreme sensitivity

Note. PWLCM = Piecewise Linear Chaotic Map; ICMIC = Iterative Chaotic Map with Infinite Collapses. Equations adapted from Xu et al. (2021) and Bingol and Alatas (2020). z(t) represents the chaotic state at iteration t. The sinusoidal map has been identified as the best-performing variant when combined with accelerated Particle Swarm Optimization (Xu et al., 2021).

Algorithm 3 Chaotic PSO using Sinusoidal Map for CNN Hyperparameter Optimization

```
Input: Search space H, swarm size N, iterations T
Output: Best hyperparameter set h_best

Initialize particles Xi and velocities Vi randomly in H
Initialize chaotic state z in (0,1)
Evaluate fitness of each particle
Set personal best Pi = Xi
Set global best G = best Pi

For t = 1 to T:
    Update chaotic sequence:
        z = a * z^2 * sin(pi * z)

    For each particle i:
        Set r1 = z
        Update chaotic sequence:
            z = a * z^2 * sin(pi * z)
        Set r2 = z

        Update velocity:
            Vi = w*Vi + c1*r1*(Pi - Xi) + c2*r2*(G - Xi)

        Update position:
            Xi = Xi + Vi

        Evaluate fitness of Xi

        If fitness(Xi) > fitness(Pi):
            Pi = Xi

    Update global best G from all Pi

Return G as h_best
```

Chaotic Particle Swarm Optimization using Sinusoidal Map for CNN Hyperparameter Optimization is an enhanced PSO where random coefficients are replaced with chaotic sequence values generated by the sinusoidal map. Improves diversity and search space coverage. Reduces premature convergence. Parameter a is typically set to 2.3. Suitable for complex, non-convex hyperparameter spaces.

The Transit Search Algorithm and Its STSOA Extension

The Transit Search (TS) algorithm, introduced by Mirrashid and Naderpour (2021), is a population-based MHA inspired by the astronomical transit method used to detect exoplanets. The algorithm operationalizes this metaphor through six mechanistic stages. In the Galaxy stage, the algorithm initializes a galaxy centre and identifies high-fitness habitable zone regions. In the Star stage, main stars are generated within each identified region using equations governed by random coefficients and noise parameters. The Transit stage calculates stellar luminosity based on positional rankings and telescope distance, comparing new and old luminosity to determine whether a transit event is detected (PT = 1) or not (PT = 0). The Planet stage, activated when PT = 1, uses signal averaging across multiple sub-signals to approximate the planet's orbital position at aphelion, perihelion, or intermediate regions governed by a zone parameter z. The Neighbour stage, activated when PT = 0, guides the search toward neighbouring stellar positions. The Exploitation stage applies a correction factor K to the best discovered planetary positions, providing local intensification.

The signal-to-noise ratio (SN) parameter governs the number of signal samples used in position estimation, providing a mechanism to balance precision and computational cost. Sensitivity analysis confirmed that the TS algorithm achieves best performance for unconstrained Optimization problems with only a 2.1% average error difference (Mirrashid & Naderpour, 2021). The Sinusoidal Chaotic Transit Search Optimization Algorithm (STSOA) extends the TS framework by replacing all pseudo-random number generation with sinusoidal chaotic sequences governed by $z(t+1) = a*z(t)^2*\sin(pi*z(t))$ with a = 2.3. Dynamic exploitation and exploration weights, adjusted as $alpha(t) = w\_exploit*(1 - t/T\_max)$ and $beta(t) = w\_explore*(t/T\_max)$, ensure that global exploration dominates in early iterations while local exploitation dominates in later stages. A chaotic global jump mechanism, activated with small probability p_jump, provides additional diversification to prevent premature convergence (Xing et al., 2024).

RESULTS

The 82 included studies were organized across three primary categorization dimensions, which are imaging modality, optimization strategy, and performance benchmarks.

Category I: CT-Based CNN Approaches

CT imaging represents the most widely studied modality for automated lung cancer detection due to its high spatial resolution and clinical accessibility. CT-focused studies predominantly addressed pulmonary nodule detection and malignancy characterization, with datasets drawn primarily from the Lung Image Database Consortium and Image Database Resource Initiative (LIDC-IDRI) repository. Table 5 summarizes selected CT-based CNN studies from the reviewed literature.

Table 5 Selected CT-Based CNN Studies for Lung Cancer Detection

Study	Architecture	Dataset	Key Metrics	Limitation
Lakshmanaprabu et al. (2019)	Optimal Deep Neural Network (ODNN)	CT scans	Accuracy: 96.2%; SEN: 94.2%; SPEC: 94.56%	No MHA; limited dataset size
Bhatia et al. (2019)	UNet+ResNet preprocessing; XGBoost+RF ensemble	LIDC-IDRI	84% improvement over typical	Ensemble; no end-to-end CNN
Kasinathan et al. (2019)	Active contour model + CNN	3D CT scans	3D tumor detection and classification	No MHA; no standard benchmark
Nithila and	SBGF-SPF active	CT images	Fast, reliable	Binary only; no MHA

ISSN No. 2321-2705 | DOI: 10.51244/IJRSI |Volume XIII Issue IV April 2026

Study	Architecture	Dataset	Key Metrics	Limitation
Kumar (2019)	contour + classifier		segmentation	
Shailesh et al. (2020)	VGG-16 + GoogLeNet	CT images	Efficient cancer region identification	Metrics not standardized
Kalaivani et al. (2020)	Deep CNN	CT images	Cancer classification achieved	Performance incompletely reported
Liu et al. (2020)	YOLOv3	CT (simulated + patient, n=888)	SEN 90.0% (simulated); 95.4% (patient); <1mm localization error	Detection only; no malignancy class.
Deepa et al. (2021)	Ridge-Adaline SGD Classifier + AI pipeline	CT nodule data	CAD sensitivity 90.0%	Minimal deep learning component
Chintakayala et al. (2022)	CNN vs. SVM binary	CT images	CNN > SVM; FPR concern noted	Binary; no hyperparameter Optimization
Zia et al. (2024)	Dual attention CNN (channel+spatial)	Benchmark nodule datasets	State-of-the-art nodule classification	No systematic hyperparameter search
Abdulqader et al. (2025)	Custom multi-task detector with transformer-based attention layers, adaptive anchor-free detection head, and improved feature pyramid network (FPN)	1608 CT images (623 cancer, 985 non-cancer)	mAP 96.26%, IoU 95.76%, precision 98.11%, recall 98.83% on held-out test set; outperforms YOLOv9 and YOLOv10 (best comparator mAP 95.70%)	Single, institutional dataset (no external validation); potential overfitting; performance only compared against YOLO-style detectors
Hosseini et al. (2025)	Hybrid CNN ensemble classifier	Multi-institutional CT dataset of 262 cases	Sensitivity 92% and CPM ~0.89 for nodule detection. Multi-site validations of CLAHE-enhanced CNN.	High computational cost, dependence on accurate segmentation, and limited validation across scanners and institutions.
Zamanidoost et al. (2025)	OMS-CNN (VGG16 composite)	LUNA16 and PN9 nodule datasets	Sensitivity 94.89% and CPM (Competition Performance Metric) 0.892; designed to better capture variable nodule sizes while controlling false positives	Relied on 2D Faster R-CNN with VGG-16-derived features plus 3D DCNN post-processing, increasing architectural and optimization complexity.

Note. LIDC-IDRI = Lung Image Database Consortium and Image Database Resource Initiative. SBGF-SPF = Selective Binary and Gaussian Filtering, new Signed Pressure Force. FPR = False Positive Rate; SEN = Sensitivity; SPEC = Specificity; SVM = Support Vector Machine; RF = Random Forest; YOLOv3 = You Only Look Once v3.

A clear methodological trajectory from manual segmentation pipelines toward fully automated deep learning architectures is observable across CT-based studies. Lakshmanaprabu et al. (2019) reported accuracy of 96.2% using an Optimal Deep Neural Network on CT images, establishing an early benchmark for automated CT classification. Bhatia et al. (2019) combined deep residual learning with UNet and ResNet preprocessing pipelines, achieving an 84% performance improvement over typical techniques on the LIDC-IDRI dataset

ISSN No. 2321-2705 | DOI: 10.51244/IJRSI |Volume XIII Issue IV April 2026

through an XGBoost and Random Forest ensemble. Liu et al. (2020) applied YOLOv3 to pulmonary nodule detection in both simulated and patient-based CT datasets, achieving detection sensitivities of 90.0% and 95.4% respectively, with nodule localization errors below 1 mm. Zia et al. (2024) proposed a bespoke CNN incorporating dual attention mechanisms to selectively weight morphologically relevant nodule features, achieving state-of-the-art accuracy on benchmark datasets, though without a systematic hyperparameter Optimization strategy. The absence of MHA integration in the majority of CT-based studies represents a significant gap given the known sensitivity of CNN performance to hyperparameter selection.

CT-based CNN research in 2025-2026 demonstrated a marked shift toward multi-modal and multi-objective architectures, combining detection, classification, and localization within unified deep learning frameworks. Abdulqader et al. (2025) proposed a multi-objective deep learning framework for CT lung cancer detection using transformer-based attention layers, adaptive anchor-free mechanisms, and an improved feature pyramid network operating on a dataset of 1,608 CT images (623 cancerous, 985 non-cancerous). The model addressed detection, classification, and localization jointly, demonstrating that multi-task Optimization confers substantial performance advantages over single-objective architectures. Hosseini et al. (2025) conducted a comparative study of preprocessing techniques, morphological segmentation, and hybrid CNN-ensemble approaches on a multi-institutional CT dataset of 262 cases collected across Iran and Iraq, providing one of the first multi-site validations of CLAHE-enhanced CNN pipelines in the reviewed literature. Zamanidoost et al. (2025) introduced the Optimized Multi-Scale CNN (OMS-CNN) for lung nodule detection, employing the Parameter-Setting-Free Harmony Search (PSF-HS) algorithm to automatically configure the number of channels in composite VGG16-derived feature layers, reporting accuracy improvements in the IEEE Journal of Biomedical and Health Informatics.

Category II: X-Ray-Based CNN Approaches

Chest X-ray imaging offers accessibility advantages in resource-constrained settings; however, its lower spatial resolution relative to CT imaging imposes greater demands on feature extraction architectures. Studies employing X-ray datasets have generally reported lower raw accuracy figures than CT-based approaches, reflecting the inherent diagnostic challenge of the modality. Table 6 presents selected X-ray-based CNN studies.

Table 6 Selected X-Ray-Based CNN Studies for Lung Cancer Detection

Study	Architecture	Dataset	Key Metrics	Notes
Ardila et al. (2019)	End-to-end 3D deep learning	NLST (low-dose CT/X-ray equivalent)	AUC 94.4%; outperformed 11 radiologists	Large-scale validation; high computational cost
Nithila and Kumar (2019)	Level set segmentation + CNN	Chest X-ray images	Fast, reliable segmentation	Limited classification metrics reported
Roy et al. (2019)	CNN vs. supervised neural network	Chest X-ray lung images	CNN outperformed SNN	Dataset size and benchmark unstandardized
Bijaya and Thapa (2020)	CNN 3-class	Histopathology + X-ray variants	Train: 96.11%; Val: 97.20%	Threshold sensitivity not evaluated
Abhishek et al. (2022)	Random Forest; SVM; KNN (ML baselines)	Lung cancer dataset	RF: 84.2%; SVM: 82.1%	No CNN; no MHA; useful ML ceiling benchmark

Note. SNN = Supervised Neural Network; SVM = Support Vector Machine; KNN = K-Nearest Neighbour; RF = Random Forest; AUC = Area Under the ROC Curve; NLST = National Lung Screening Trial; Train = training accuracy; Val = validation accuracy.

Ardila et al. (2019) presented a landmark end-to-end deep learning system applied to low-dose CT screening data from the National Lung Screening Trial, achieving an AUC of 94.4% and surpassing the performance of 11 radiologists in a controlled reader study. Roy et al. (2019) demonstrated that CNN architectures consistently

ISSN No. 2321-2705 | DOI: 10.51244/IJRSI |Volume XIII Issue IV April 2026

outperformed supervised neural networks on chest X-ray lung cancer classification. Abhishek et al. (2022) provided a critical machine learning baseline comparison, reporting Random Forest accuracy of 84.2% and SVM accuracy of 82.1% on the same dataset. This is a performance ceiling substantially exceeded by all Optimized CNN architectures reviewed, confirming the value of deep learning for automated lung cancer diagnosis.

Category III: Histopathology-Based CNN Approaches

Histopathological image classification represents the most clinically definitive diagnostic modality and has attracted growing attention in the deep learning literature following the availability of annotated public datasets. Classification tasks in this category involve distinguishing among Malignant, including adenocarcinoma and squamous cell carcinoma subtypes; Benign; and Normal tissue categories from hematoxylin and eosin-stained slides. Table 7 summarizes selected histopathology-based CNN studies.

Table 7 Selected Histopathology-Based CNN Studies for Lung Cancer Classification

Study	Model	Dataset (n)	Accuracy (%)	Classes	Optimization
Narmada et al. (2019)	CNN with softmax	Histopathology slides	95.00	Multi	Architecture selection
Ponnada and Srinivasu (2019)	EFFI-CNN (7-layer)	Histopathology slides	Best vs ICDSSPLD-CNN, EASPLDCNN	Multi	Architecture design
Bijaya and Thapa (2020)	Standard CNN	Histopathology (3-class)	97.20 (val)	3	None
Rao et al. in Chintakayala et al. (2022)	Standard CNN	CT (71 patients)	76.0	Binary	None
Rossetto and Zhou in Chintakayala et al. (2022)	Deep learning	CT (1,500 patients; 150,000 slices)	97.0	Binary	None (scale compensates)
Jim et al. (2025)	Lightweight CNN, 4 convolutional layers, ~3M parameters with integrated XAI (Saliency Maps, Grad-CAM).	LC25000 histopathology lung cancer image dataset.	99.62 (epoch time ≈ 60s, very low computational cost).	Multi	Single public dataset; limited testing on diverse scanners/labs and real clinical workflows.
Usman et al. (2025)	Fine-tuned VGG-16 with wavelet transform; hyperparameters optimized via CL-PSO; ensemble classification.	IQ-OTH/NCCD lung CT dataset.	99.99	Multi	Near-perfect performance on a single dataset risks overfitting; limited external validation and clinical robustness analysis.
Mathivanan et al. (2025)	Superpixel-guided preprocessing; deep feature fusion from ResNet-50/101/152; feature selection via PSO and Red Deer Optimization.	Histopathological lung cancer images (multi-class classification).	≈90–100% accuracy across classifiers under K-fold cross-validation.	Multi	Complex multi-stage pipeline; potential overfitting and limited evidence of performance on external histology cohorts.

ISSN No. 2321-2705 | DOI: 10.51244/IJRSI |Volume XIII Issue IV April 2026

Note. EFFI-CNN = Efficient CNN. val = validation set. T = decision threshold. Rao et al. and Rossetto & Zhou figures cited from related works reviewed in Chintakayala et al. (2022).

A clear performance gradient is observable across histopathology-based studies when ranked by Optimization sophistication. The performance increase from Bijaya and Thapa (2020) (standard CNN, 97.20% validation accuracy) to STSOA-CNN (98.88% test accuracy at threshold 0.75) represents a direct benefit of metaheuristic hyperparameter Optimization with sinusoidal chaotic enhancement. The comparison between the small-dataset CNN (76% accuracy, n=71 patients) and the large-dataset deep learning model (97% accuracy, n=1,500 patients) cited in Chintakayala et al. (2022) illustrates the well-established data dependency of unoptimized CNN performance.

Histopathology-focused studies in 2025 demonstrated particularly strong performance, with several achieving accuracy figures exceeding 99% through Optimized lightweight architectures. Jim et al. (2025) introduced the Explainable and Lightweight Lung Cancer Net (XLLC-Net), a four-convolutional-layer CNN containing only 3 million parameters that achieved 99.62% classification accuracy on the LC25000 histopathology dataset with Saliency Map and Grad-CAM explainability. Critically, XLLC-Net completed each training epoch in 60 seconds, establishing a new benchmark for computationally efficient histopathology CNN design. The model's integration of XAI directly into the lightweight architecture addresses two of the most persistent gaps identified in the primary review simultaneously. Usman et al. (2025) proposed an ensemble transfer learning framework combining a fine-tuned VGG-16 architecture with Comprehensive Learning Particle Swarm Optimization (CL-PSO) for automatic hyperparameter tuning on the IQ-OTH/NCCD lung CT dataset. CL-PSO enhanced diversity through comprehensive learning strategies that prevent particles from converging prematurely, and the framework achieved near-perfect classification accuracy of 99.99%, with Grad-CAM visualizations confirming radiologically coherent decision regions. Mathivanan et al. (2025) applied a superpixel-guided ResNet framework with PSO and Red Deer Optimization (RDO) for feature selection from fused ResNet-50, ResNet-101, and ResNet-152 features in histopathology lung cancer classification. The combination of particle swarm-guided feature selection with multi-scale ResNet feature fusion demonstrated 90-100% accuracy across multiple classifiers in K-fold cross-validation.

Category IV: Metaheuristic Optimization Strategies

The reviewed literature documents a progressive diversification of Optimization strategies applied to CNN hyperparameter selection. Table 8 categorizes the principal Optimization paradigms identified, with representative algorithms, applications, and performance outcomes.

Table 8 Metaheuristic Optimization Paradigms Applied to CNN Hyperparameter Tuning

Paradigm	Algorithms	CNN Application	Reported Benefit	Representative Studies
Swarm-based	PSO, ACO, ABC, Tuna Swarm Optimization	Filter size; learning rate; layer depth	Improved convergence; reduced training time	Wang et al. (2021); Xie et al. (2021)
Evolutionary	Genetic Algorithm, Differential Evolution, Evolutionary Strategies	Neural architecture search; weight initialization	Global optima discovery; avoidance of local minima	Dokeroglu et al. (2019); Yang (2020)
Physics-inspired	Simulated Annealing; Gravitational Search Algorithm	Regularization tuning; network pruning	Probabilistic escape from local optima	Wang et al. (2021); Shan et al. (2021)
Chaotic-enhanced MHA	Chaotic PSO; Chaotic ACO; Chaotic DE	Hyperparameter diversity; search space coverage	Faster convergence; reduced local optima trapping	Bingol and Alatas (2020); Zhao et al. (2021)

Paradigm	Algorithms	CNN Application	Reported Benefit	Representative Studies
Transit Search	TSOA-CNN; STSOA-CNN	Learning rate, layers, filter size for lung cancer CNN	98.88% accuracy; 37% time reduction vs. CNN	Mirrashid and Naderpour (2021); Xing et al. (2024)

Note. PSO = Particle Swarm Optimization; ACO = Ant Colony Optimization; ABC = Artificial Bee Colony; DE = Differential Evolution; TSOA-CNN performance reported at threshold 0.75 for Malignant classification. 37% time reduction is relative to standard CNN baseline.

Category V: Chaotic Map Integration in CNN Optimization

Among the 12 chaotic map variants catalogued in Table 4, the sinusoidal, logistic, and tent maps have attracted the greatest application frequency in the reviewed studies. Xu et al. (2021) conducted a comparative study of all twelve maps combined with Grey Wolf Optimization across multiple benchmark datasets, establishing that the sinusoidal map consistently provided the best Optimization performance due to its non-uniform probability distribution and concentrated mid-range sampling properties. Bingol & Alatas (2020) demonstrated that chaotic optics-inspired algorithms incorporating chaotic sequences universally outperformed their pseudo-random counterparts on global Optimization benchmarks, with improvements of 5-15% in convergence speed across problem categories.

Zhao et al. (2021) demonstrated that chaotic random spare Ant Colony Optimization substantially improved multi-threshold image segmentation performance, a result that generalizes to the feature extraction problem in lung cancer classification. The STSOA-CNN framework, which employs the sinusoidal map z(t+1) = a*z(t)^2*sin(pi*z(t)) with a = 2.3 to generate exploration coefficients and initialize the search population, achieved the highest accuracy values across all three tissue categories in the reviewed literature. The chaotic global jump mechanism in STSOA-CNN, activated with small probability p_jump at each iteration, provided a critical diversification mechanism that distinguished STSOA-CNN from TSOA-CNN, particularly in its ability to recover from stagnation in low-gradient fitness regions and maintain high sensitivity for the minority Benign class.

Preprocessing Pipelines Across the Reviewed Literature

The reviewed literature documents substantial heterogeneity in preprocessing strategies, a factor that exerts significant influence on reported classification performance. CT-based studies employed preprocessing pipelines including Hounsfield unit windowing for tissue contrast enhancement, morphological operations for nodule boundary delineation, and active contour models for region-of-interest extraction (Kasinathan et al., 2019; Nithila & Kumar, 2019). Histopathology-based studies applied colour normalization, stain deconvolution, and patch extraction to address the high spatial resolution and colour variability of haematoxylin and eosin-stained slides.

The preprocessing pipeline of the STSOA-CNN framework demonstrated particular systematic rigour, incorporating five sequential stages: greyscale conversion with pixel intensity mapping to [0, 255], Contrast Limited Adaptive Histogram Equalization (CLAHE) for localized tissue contrast enhancement through non-overlapping tile-based histogram equalization, intensity normalization to the [0, 1] range, morphological thinning for noise removal while preserving topological structure, and Fuzzy C-means (FCM) clustering for probabilistic ROI segmentation (Alam et al., 2025; Islam et al., 2024; Sharma et al., 2023; Sujatha et al., 2025). FCM's probabilistic membership assignment is particularly suited to medical images characterized by gradual intensity transitions at tissue boundaries. Image augmentation through scaling, rotation, and shearing was applied to the training partition to improve model generalization across the class-imbalanced dataset.

Swarm-Optimized and Hybrid MHA-CNN Studies

The reviewed recent literature documents a proliferation of swarm-Optimized CNN architectures with significantly more sophisticated hybridization strategies. Omprakash and Samiappan (2025) introduced

ISSN No. 2321-2705 | DOI: 10.51244/IJRSI |Volume XIII Issue IV April 2026

LungSwarmNet, a DenseNet201 architecture Optimized with PSO for multi-class lung cancer classification from CT scans, combined with ResNet50 for segmentation. The PSO-DenseNet201 classifier used a fitness function to rank candidate feature combinations and correctly identified Squamous Cell Carcinoma, Adenocarcinoma, and Normal classes in a three-class configuration. The Flower Pollination Algorithm (FPA) emerged as a notable new Optimizer in this literature period. Altuhaifa and Albedah (2025) demonstrated that FPA-based adaptive weight Optimization for an ensemble of VGG16, ResNet101V2, and InceptionV3 architectures substantially outperformed static ensemble weighting and PSO-based ensemble approaches for CT lung cancer classification. Raghuvanshi et al. (2024) reported that the hybrid PSbBO-Net, which fuses PSO with Bayesian Optimization around a Gaussian Process surrogate model to tune DenseNet hyperparameters, achieved 99.5% accuracy on histopathological images and 98.8% accuracy on lung CT images, establishing a new state of the art for the PSO-based MHA-CNN paradigm.

Sabri et al. (2025) proposed an enriched lung cancer classification framework combining Hybrid Horse Herd Optimization (HHO) with the Lion Optimization Algorithm (LOA) for feature extraction and refinement, coupled with a Deep Convolutional Neural Network and Long Short-Term Memory (DCNN + LSTM) classifier. The framework applied adaptive filters for preprocessing and demonstrated that the HHO-LOA hybrid provided superior feature selection relative to single-algorithm Optimization baselines. A related study by Prasad et al. (2024) proposed a Hybrid Spotted Hyena Optimization combined with Seagull Algorithm for feature selection applied to CNN-LSTM classification on LIDC/IDRI and chest X-ray datasets, using DCGAN-based data augmentation to address class imbalance, achieving competitive performance in Soft Computing. Studies also documented the Slime Mould Algorithm (SMA) as an effective hyperparameter Optimizer. CNN feature extraction guided by SMA combined with the Squeeze-Inception-ResNeXt classifier achieved 97.7% accuracy, 98.1% sensitivity, and 97.4% specificity on three-class lung disease classification (Kaur et al., 2025).

Explainability-Integrated CNN Studies

Recent literature witnessed the systematic integration of explainability mechanisms directly into CNN-based lung cancer frameworks, a trend that is absent from earlier studies. Hammad et al. (2025) combined a custom CNN with Grad-CAM to classify lung cancer CT images into squamous cell carcinoma, large cell carcinoma, and adenocarcinoma, demonstrating that Grad-CAM activation maps aligned with histologically recognized tissue regions for correct classifications while revealing diagnostic error patterns for misclassified cases. The study achieved 93.06% overall accuracy with high precision, recall, and F1-scores across all three subtypes. LCxNet (Hussain et al., 2025) introduced a custom CNN framework systematically evaluated across five Optimizers — SGD, RMSProp, Adam, AdamW, and NAdam — integrated with Grad-CAM decision visualization and t-SNE feature space analysis, achieving 99.39% accuracy, 99.45% specificity, and AUC of 1.00 on the IQ-OTH/NCCD benchmark, outperforming all previously reported results on that dataset. Jim et al. (2025) demonstrated through XLLC-Net that Saliency Map visualizations consistently highlighted nuclear architecture, cellular density, and glandular formation as the primary classification drivers. These features directly aligned with pathological diagnostic criteria, thereby providing interpretable evidence that the model's feature learning corresponds to medically grounded representations.

The emergence of this XAI-integrated CNN cohort in recent years directly addresses one of the most significant gaps identified in the primary systematic review, which is the absence of clinician-interpretable model outputs as a barrier to clinical deployment. The convergence of high classification accuracy (93.06-99.99%) with meaningful post-hoc explanations in multiple recent studies suggests that the field is approaching a critical threshold for clinical translation. Critically, however, none of the reviewed XAI-integrated studies combined explainability mechanisms with metaheuristic hyperparameter optimization, representing the most important unfilled research gap at the close of the review period.

Table 9 summarizes emerging recent literature on CNN approaches for lung cancer detection, stating their key contributions.

ISSN No. 2321-2705 | DOI: 10.51244/IJRSI |Volume XIII Issue IV April 2026

Table 9 Summary of Emerging Recent Literature on CNN Approaches for Lung Cancer Detection

Study	Modality	Architecture	Optimization	Accuracy (%)	Key Contribution
Raghuvanshi et al. (2024)	CT/Histopathology	PSbBO-Net (DenseNet+GAN)	PSO + Bayesian Optimization (GP surrogate)	99.5 (hist.); 98.8 (CT)	PSO-BO fusion achieves state-of-the-art MHA-CNN; GP model refines particles
Abdulqader et al. (2025)	CT	Transformer attention + feature pyramid	Adaptive anchor-free mechanism	NR	Multi-objective detection, classification and localization in one framework
Altuhaifa and Albedah (2025)	CT	VGG16+ResNet101V2+InceptionV3 ensemble	Flower Pollination Algorithm (FPA)	NR (best vs PSO/BO)	FPA adaptively Optimizes ensemble weights; outperforms static and PSO weighting
Farghali et al. (2025)	CT/Histopathology	Optimized SCNN	Sequential architecture tuning	NR	Reduced computation complexity; faster inference than standard CNN
Hammad et al. (2025)	CT	Custom CNN + Grad-CAM (XAI)	Multi-optimizer evaluation	93.06	3-subtype classification; Grad-CAM aligns with histological tissue markers
Hosseini et al. (2025)	CT	CNN-ensemble + transfer learning	CLAHE preprocessing comparison	NR	Multi-institutional validation across Iran and Iraq; CLAHE shown critical
Hussain et al. (2025)	CT	LCxNet CNN + t-SNE	5 optimizers compared (Adam, SGD, etc.)	99.39 (AUC=1.00)	Grad-CAM visualization; best IQ-OTH/NCCD benchmark reported to date
Jim et al. (2025)	Histopathology	XLLC-Net (4-conv lightweight CNN)	Architecture minimization	99.62	3M parameters; 60s/epoch; Grad-CAM + Saliency Map; LC25000 benchmark
Kaur et al. (2025)	CT	CNN + Squeeze-Inception-ResNeXt	Slime Mould Algorithm (SMA)	97.7	SMA Optimizes feature extraction; 3-class lung disease classification
Omprakash and Samiappan (2025)	CT	LungSwarmNet (ResNet50 + DenseNet201+PSO)	Particle Swarm Optimization	Competitive	PSO-guided fitness ranking for 3-class CT classification
Sabri et al. (2025)	CT/X-ray	DCNN + LSTM	Hybrid HHO + LOA	NR	HHO-LOA hybrid feature Optimization; joint temporal-spatial classification
Shukla et al. (2025)	CT	ILN-TL-DM (P-ResU-Net + transfer learning)	Chaotic Crow Search Algo. + RF (CCSA-RF)	NR (high)	Hybrid radiomic + attention DL; 97.5% accuracy with SCNN-PNN variant cited
Usman et al. (2025)	CT	VGG-16 + Wavelet Transform Eq.	CL-PSO (comprehensive learning PSO)	99.99	Near-perfect IQ-OTH/NCCD accuracy; Grad-CAM validates radiological decisions
Zamanidoost et al. (2025)	CT	OMS-CNN (VGG16 composite)	PSF-HS Harmony Search	NR	Automatic multi-scale feature map configuration; first PSF-HS lung CNN

ISSN No. 2321-2705 | DOI: 10.51244/IJRSI |Volume XIII Issue IV April 2026

Note. NR = Not Reported or not standardized for comparison; Hist = Histopathology; PSF-HS = Parameter-Setting-Free Harmony Search; OMS-CNN = Optimized Multi-Scale CNN; ILN-TL-DM = Improved Learned Network Transfer Learning Deep Model; CCSA-RF = Chaotic Crow Search Algorithm with Random Forest; HHO = Horse Herd Optimization; LOA = Lion Optimization Algorithm; SMA = Slime Mould Algorithm; CL-PSO = Comprehensive Learning Particle Swarm Optimization; PSbBO = Particle Swarm Bayesian Optimization; GAN = Generative Adversarial Network; FPA = Flower Pollination Algorithm. Studies are cited as reported in the respective publications

Performance Benchmark Synthesis

This section synthesizes the quantitative performance data extracted from reviewed studies, enabling direct comparison across imaging modalities, model types, and Optimization strategies. Table 10 presents a consolidated benchmark comparison for studies reporting standardized classification metrics, and Table 11 presents the comprehensive threshold-level evaluation for the three CNN architectures at the centre of the transit search-based Optimization literature.

Table 10 Consolidated Performance Benchmarks Across Selected Studies (2019-2026)

Study	Modality	Model Type	Classes	Accuracy (%)	SEN (%)	SPEC (%)	MHA Used
Lakshmana prabu et al. (2019)	CT	ODNN	Binary	96.20	94.20	94.56	None
Bhatia et al. (2019)	CT	ResNet+UNet+Ensemble	Binary	84.0 (gain)	NR	NR	None
Ardila et al. (2019)	Low-dose CT	End-to-end DL	Binary	AUC=94.4	NR	NR	None
Kasinathan et al. (2019)	CT	Active Contour+CNN	Multi-class	NR	NR	NR	None
Narmada et al. (2019)	Histopathology	CNN (softmax)	Multi-class	95.00	NR	NR	Arch. tuning
Ponnada and Srinivasu (2019)	Histopathology	EFFI-CNN	Multi-class	Best in class	NR	NR	Arch. design
Roy et al. (2019)	X-ray	CNN vs. SNN	Binary	CNN > SNN	NR	NR	None
Bijaya and Thapa (2020)	Histopathology	Standard CNN	3-class	97.20 (val)	NR	NR	None
Shailesh et al. (2020)	CT	VGG-16+GoogLeNet	Multi-class	Not standardized	NR	NR	None
Deepa et al. (2021)	CT	Ridge-Adaline SGD	Detection	NR	90.0	NR	SGD
Liu et al. (2020)	CT	YOLOv3	Detection	NR	95.4 (patient)	NR	None
Abhishek et al. (2022)	CT/X-ray	Random Forest (best)	Multi-class	84.20	NR	NR	None
Chintakayal	CT	CNN (binary)	Binary	CNN >	NR	NR	None

Study	Modality	Model Type	Classes	Accuracy (%)	SEN (%)	SPEC (%)	MHA Used
a et al. (2022)				SVM			
Zia et al. (2024)	CT	Dual Attention CNN	Multi-class	SOTA	NR	NR	None
Raghuvanshi et al. (2024)	Histopathology	PSbBO-Net (DenseNet+GAN)	Multi	99.5 (hist); 98.8 (CT)	99.2	NR	PSO + Bayesian Optimization
Jim et al. (2025)	Histopathology	XLLC-Net (lightweight)	3-class	99.62	99.67	NR	Architecture minimisation
Usman et al. (2025)	CT	VGG-16 + CL-PSO	3-class	99.99	99.98	NR	Comprehensive Learning PSO
Hussain et al. (2025)	CT	LCxNet (multi-optim.)	3-class	99.39	NR	99.45	Multi-optimizer + Grad-CAM
Kaur et al. (2025)	CT	Squeeze-Inception-ResNeXt + SMA	3-class	97.7	98.1	97.4	Slime Mould Algorithm
Omprakash and Samiappan, (2025)	CT	LungSwarmNet (DenseNet+PSO)	3-class	Compet.	NR	NR	Particle Swarm Optimization
Hammad et al. (2025)	CT	Custom CNN + Grad-CAM	3-class	93.06	NR	NR	Multi-optim.; Grad-CAM XAI
Hosseini et al. (2025)	CT	CNN-ensemble + ResNet, VGG16, Xception	Binary	NR	NR	NR	CLAHE + transfer learning
Zamanidoost et al. (2025)	CT	OMS-CNN	Detection	NR	Improved	NR	PSF-HS Harmony Search
Sabri et al. (2025)	CT	DCNN + LSTM + HHO-LOA	Multi	NR	NR	NR	Hybrid Horse Herd + Lion Opt.
Altuhaifa and Albedah (2025)	CT	VGG16+ResNet101V2+InceptionV3	Multi	NR (best ensemble)	NR	NR	Flower Pollination Algorithm
TSOA-CNN	Histopathology	Transit Search CNN	3-class	97.54	97.50	97.57	Transit Search
STSOA-CNN	Histopathology	Sinusoidal Chaotic TS-CNN	3-class	98.88	98.81	98.94	Sin. Chaotic TS

Note. NR = Not Reported; SOTA = State of the Art (specific value not publicly reported); val = validation set; AUC = Area Under the ROC Curve; NR = Not Reported or not standardized. Compet. = competitive but exact figure not reported in comparable form. SEN = Sensitivity; SPEC = Specificity; ODNN = Optimal Deep Neural Network; EFFI-CNN = Efficient CNN; SNN = Supervised Neural Network; SGD = Stochastic Gradient Descent. PSF-HS = Parameter-Setting-Free Harmony Search; HHO = Horse Herd Optimization; LOA = Lion Optimization Algorithm; SMA = Slime Mould Algorithm; CL-PSO = Comprehensive Learning PSO. For comparison, STSOA-CNN from the primary review achieved 98.88% accuracy, 98.81% SEN, 98.94% SPEC on the Malignant class at threshold 0.75 (histopathology dataset, n=3,291).

ISSN No. 2321-2705 | DOI: 10.51244/IJRSI |Volume XIII Issue IV April 2026

Table 11 Cross-Model, Cross-Class Performance Comparison at Selected Thresholds: CNN vs. TSOA-CNN vs. STSOA-CNN

Class	Model	Threshold	FPR (%)	SPEC (%)	SEN (%)	ACC (%)	Time (s)
Malignant	STSOA-CNN	0.25	1.55	98.45	98.99	98.72	57.86
Malignant	STSOA-CNN	0.50	1.18	98.82	98.87	98.85	57.37
Malignant	STSOA-CNN	0.75	1.06	98.94	98.81	98.88	57.51
Malignant	TSOA-CNN	0.25	2.92	97.08	97.68	97.39	76.88
Malignant	TSOA-CNN	0.50	2.55	97.45	97.56	97.51	76.28
Malignant	TSOA-CNN	0.75	2.43	97.57	97.50	97.54	76.61
Malignant	CNN	0.25	3.92	96.08	96.73	96.41	91.03
Malignant	CNN	0.50	3.54	96.46	96.61	96.54	91.56
Malignant	CNN	0.75	3.42	96.58	96.55	96.57	91.02
Benign	STSOA-CNN	0.25	0.89	99.11	95.00	98.66	54.53
Benign	STSOA-CNN	0.50	0.68	99.32	94.44	98.78	53.60
Benign	STSOA-CNN	0.75	0.61	99.39	94.17	98.81	53.59
Benign	TSOA-CNN	0.25	1.54	98.46	89.72	97.51	72.83
Benign	TSOA-CNN	0.50	1.33	98.67	89.17	97.63	72.57
Benign	TSOA-CNN	0.75	1.26	98.74	88.89	97.66	72.40
Benign	CNN	0.25	2.05	97.95	85.56	96.60	90.65
Benign	CNN	0.50	1.84	98.16	85.00	96.72	89.29
Benign	CNN	0.75	1.77	98.23	84.72	96.75	90.10
Normal	STSOA-CNN	0.25	1.32	98.68	98.48	98.60	57.19
Normal	STSOA-CNN	0.50	1.03	98.97	98.32	98.72	55.71
Normal	STSOA-CNN	0.75	0.93	99.07	98.24	98.75	56.31
Normal	TSOA-CNN	0.25	2.25	97.75	96.96	97.45	75.41
Normal	TSOA-CNN	0.50	1.96	98.04	96.79	97.57	74.40
Normal	TSOA-CNN	0.75	1.86	98.14	96.71	97.60	74.57
Normal	CNN	0.25	2.99	97.01	95.75	96.54	88.41
Normal	CNN	0.50	2.69	97.31	95.59	96.66	88.19
Normal	CNN	0.75	2.59	97.41	95.51	96.69	89.43

Note. FPR = False Positive Rate; SPEC = Specificity; SEN = Sensitivity; ACC = Accuracy. Source dataset: 3,291 histopathology images (Malignant n=1,683; Benign n=360; Normal n=1,248) from Kaggle/Mendeley Data. Threshold 0.36 omitted for conciseness; values follow the same monotonic trend. Computation time includes training, testing, and validation phases.

Several key patterns emerged from the benchmark synthesis in Tables 10 and 11. First, across all three tissue categories and all four decision thresholds, STSOA-CNN achieves the lowest FPR values, highest specificity and sensitivity, highest accuracy, and fastest computation times relative to both TSOA-CNN and standard CNN. Second, the performance increment from standard CNN to TSOA-CNN is consistent and positive across all metrics, confirming the value of transit search Optimization as a standalone strategy. However, the increment from TSOA-CNN to STSOA-CNN is larger in magnitude for sensitivity and FPR, suggesting that the sinusoidal chaotic enhancement contributes disproportionately to classification robustness. Third, the Benign class exhibits the largest inter-model performance differential for sensitivity, a gap of 10.28 percentage points between STSOA-CNN (95.00%) and standard CNN (84.72%) at threshold 0.25, which reflects the chaotic optimizer's superior handling of the class imbalance inherent in the 10.9% Benign representation in the dataset. Fourth, STSOA-CNN computation times are approximately 37% lower than standard CNN across all

ISSN No. 2321-2705 | DOI: 10.51244/IJRSI |Volume XIII Issue IV April 2026

categories, a direct consequence of hyperparameter optimization selecting more computationally efficient CNN configurations.

Table 12 presents the meta-analytic statistical aggregation across 23 studies with fully quantitative reported accuracy values. Studies with only qualitative descriptors (SOTA, CNN>SVM) were excluded from the statistical summary. Means and standard deviations are calculated from reported test-set accuracy figures; ranges reflect the minimum and maximum values within each stratum.

Table 12 Meta-Analytic Statistical Aggregation of Accuracy by Modality and Optimization Category (n=23 Studies)

Stratum	n (studies)	Mean Acc. (%)	SD (%)	Min (%)	Max (%)	Interpretation
All included (quantitative)	23	97.1	2.3	84.2	99.99	MHA-CNN superior to ML baselines across modalities
CT — No optimization	7	93.6	3.1	84.2	96.2	Data-dependent; sensitive to dataset scale
CT — Single MHA	5	97.3	1.4	95.0	99.39	Consistent improvement over unoptimized baseline
CT — Hybrid MHA	4	99.5	0.4	99.06	99.99	Near-perfect accuracy; PSO-hybrids dominate
Histopathology — No optimization	3	96.7	1.1	95.0	97.20	Strong but sensitive to class imbalance
Histopathology — Chaotic/TS MHA	3	98.5	0.7	97.54	99.5	STSOA-CNN best chaotic; PSbBO-Net best PSO-hybrid
Histopathology — Lightweight CNN	1	99.62	N/A	99.62	99.62	XLLC-Net: 3M params; 60s epoch
X-ray — No optimization	2	90.2	8.5	84.2	94.4	Wide variance; dataset scale dominant factor
Unoptimized baselines (ML only)	3	83.9	1.9	82.1	86.0	Clear performance ceiling vs optimized CNNs

Note. Acc = Accuracy; SD = Standard Deviation; N/A = Single study (no SD calculable). Hybrid MHA includes PSO-Bayesian, CL-PSO, and FPA approaches. Chaotic/TS MHA includes STSOA-CNN, TSOA-CNN, CCSA-RF, and SMA-based studies. Studies with only qualitative accuracy descriptors (SOTA, CNN>SVM) excluded. AUC-reported studies (Ardila et al., 2019) included at the AUC value as a comparable metric. These statistics are descriptive summaries; formal meta-analysis is constrained by dataset heterogeneity and incomplete metric reporting across the full 82-study corpus.

DISCUSSION

The discussion synthesizes the theoretical and clinical implications of these findings, identifies the emerging trends documented in recent studies (2025-2026), and provides an expanded treatment of real-world deployment challenges.

Modality-Specific Trends

CT-based studies dominate numerically and methodologically, reflecting the availability of the LIDC-IDRI benchmark and decades of CAD development. The modality trajectory, from Nithila and Kumar (2019) and Kasinathan et al. (2019), through YOLOv3 detection (Liu et al., 2020) to multi-objective XAI-integrated frameworks (Abdulqader et al., 2025; Hussain et al., 2025; Zia et al., 2024), represents a seven-year progression from computer-aided detection to clinician-grade diagnostic support. The meta-analytic data in Table 12 confirm that the CT modality mean accuracy gap between unoptimized approaches (93.6%,

ISSN No. 2321-2705 | DOI: 10.51244/IJRSI |Volume XIII Issue IV April 2026

SD=3.1%) and hybrid MHA approaches (99.5%, SD=0.4%) is 5.9 percentage points, with a substantial variance reduction indicating that hybridization reduces performance sensitivity. Histopathology-based approaches have achieved the fastest accuracy gains in the review period, driven by the availability of LC25000 and Kaggle/Mendeley datasets and the MHA-optimized frameworks applied to them. Ardila et al. (2019) demonstrated that large-scale CT-based deep learning can achieve radiologist-level performance, but the computational resources required for such systems limit their accessibility in lower-resource clinical settings, a concern particularly relevant for African and Asian healthcare contexts.

Histopathology-based approaches, representing the diagnostic gold standard, have received comparatively less attention in the reviewed period, possibly owing to dataset availability constraints and the high-resolution demands of whole-slide image analysis. The availability of the publicly accessible Kaggle/Mendeley histopathology dataset (n = 3,291) used in the STSOA-CNN evaluation represents a useful benchmark, though its scale remains modest relative to CT imaging repositories. Across all modalities, a consistent finding emerges: dataset size and quality exert disproportionate influence on reported performance. The dramatic accuracy difference between the 71-patient dataset (76% accuracy) and the 1,500-patient dataset (97% accuracy) cited in Chintakayala et al. (2022) illustrates the data dependency inherent in unoptimized deep learning frameworks, and motivates the design of Optimization strategies that can extract maximum performance from smaller, class-imbalanced datasets.

Evolution of Optimization Strategies

The reviewed literature documents a clear evolutionary trajectory in Optimization sophistication. Studies published in 2019-2020 relied primarily on architectural design choices, activation function selection, and manual learning rate specification as implicit Optimization strategies. The period 2020-2022 saw the emergence of formal MHA-based hyperparameter Optimization, with swarm-based and evolutionary approaches demonstrating consistent performance improvements over manual configuration. The 2022-2026 period introduced chaotic-enhanced and transit search-based variants that represent the current state of the art on the histopathology classification benchmark.

The Transit Search Algorithm occupies a distinctive position in this evolutionary narrative. Unlike PSO and GA variants, which require careful tuning of their own algorithm-level parameters, the TS algorithm's astronomical metaphor provides a physically motivated mechanism for adaptive exploration-exploitation balancing through the luminosity-based transit detection mechanism (Mirrashid & Naderpour, 2021). Xing et al. (2024) demonstrated that further enhancement of TS through oscillation exploitation factors and Roche limit-inspired boundary conditions improved performance on engineering optimization problems, a finding whose implications for deep learning hyperparameter Optimization merit further investigation.

The Role of Chaotic Maps

The mathematical properties of chaotic maps provide a principled explanation for their performance advantages in MHA-CNN integration. The ergodicity property ensures that chaotic sequences eventually visit every region of the feasible hyperparameter space, providing theoretical coverage guarantees absent from pseudo-random sampling. The sensitivity to initial conditions means that small variations in the seed produce drastically different trajectories, preventing the population from clustering in locally optimal regions (Bingol & Alatas, 2020).

Among the 12 chaotic maps evaluated in the literature, the sinusoidal map demonstrates a probability distribution concentrated toward the centre of its domain. This property is particularly beneficial for hyperparameter search in neural network contexts where moderate values of learning rate and filter size tend to produce better-generalizing models than extreme values. The empirical performance gains reported for STSOA-CNN, a 1.34 percentage point improvement in accuracy over TSOA-CNN for malignant classification and a 5.28 percentage point improvement in sensitivity for benign classification, confirm that the theoretical advantages of the sinusoidal map translate directly to classification performance in the clinical application context.

ISSN No. 2321-2705 | DOI: 10.51244/IJRSI |Volume XIII Issue IV April 2026

The PSO Hybridization Wave

The 2025-2026 cohort documents an unmistakable escalation of PSO hybridization as the dominant optimization paradigm. Whereas the primary review literature (2019-2024) featured PSO primarily as a standalone swarm-based optimizer, the 2025-2026 studies document systematic hybridization with Bayesian surrogate models (Raghuvanshi et al., 2024), comprehensive learning strategies (Usman et al., 2025), Flower Pollination Algorithms (Altuhaifa & Albedah, 2025), and Red Deer Optimization (Mathivanan et al., 2025). The PSbBO-Net framework of Raghuvanshi et al. (2024), which uses a Gaussian Process model to provide probabilistic guidance for PSO particle movement, represents the most theoretically sophisticated MHA-CNN integration approach identified across the entire review period, achieving 99.5% histopathological classification accuracy. This trajectory suggests that pure single-algorithm MHA approaches are being superseded by principled hybrid frameworks that combine the global search capabilities of swarm intelligence with the probabilistic efficiency of surrogate-based optimization.

Lightweight Architecture as a Research Priority

A second major trend emerging in 2025-2026 is the explicit prioritization of computational efficiency as a design objective alongside classification accuracy. XLLC-Net's achievement of 99.62% accuracy with only 3 million parameters and a 60-second epoch time (Jim et al., 2025) represents a direct response to the resource-constrained deployment limitation identified in the primary review. This finding is clinically consequential. If lightweight architectures maintain accuracy competitive with computationally intensive models, the principal remaining barrier to deployment in African and Asian clinical settings becomes dataset availability and validation rather than hardware requirements. The combination of lightweight CNN design with metaheuristic hyperparameter optimization, as yet not demonstrated in the 2025-2026 cohort, represents the most impactful potential research contribution for improving access to AI-based lung cancer diagnosis in resource-constrained environments.

XAI Integration as a Clinical Requirement

The systematic integration of Grad-CAM, Saliency Maps, and SHAP into CNN frameworks in 2025-2026 (Hammad et al., 2025; Jim et al., 2025; Usman et al., 2025) confirms that the XAI gap identified in the primary review is now actively being addressed. However, a critical limitation remains: all XAI-integrated CNN studies in 2025-2026 implemented explainability as a post-hoc analytical layer applied after model training, rather than as an intrinsic component of the architecture design or optimization objective. The convergence of XAI with metaheuristic optimization, which optimizes not just for classification accuracy but also for explanation fidelity, represents a genuinely novel research direction with direct clinical relevance. None of the 82 studies included in the updated review addressed this convergence, thereby confirming it as an open, high-priority research gap.

Multi-Institutional Validation Begins to Emerge

Hosseini et al. (2025) stands out in the 2025-2026 cohort as one of the very few studies to collect data from geographically diverse medical centres, specifically from institutions across Iran and Iraq, providing a multi-institutional validation of the CLAHE-enhanced CNN preprocessing pipeline. While this represents meaningful progress toward the external validation gap identified in Table 12, the geographic scope remains limited to two countries within the same macro-region. No study in the 2025-2026 cohort provides validation across multiple continents, and none explicitly targets African clinical datasets, confirming that the Global South validation gap remains substantially unaddressed at the close of the review period.

Research Gaps and Limitations of Reviewed Literature

The systematic review identifies several persistent limitations that constrain the clinical translation of the reviewed frameworks. Table 13 presents the consolidated research gap analysis with evidence assessment from the full 2019-2026 period.

ISSN No. 2321-2705 | DOI: 10.51244/IJRSI |Volume XIII Issue IV April 2026

Table 13 Consolidated Research Gap Analysis with 2025-2026 Evidence Assessment

Limitation	2025-2026 Evidence Status	Clinical Impact	Research Direction	Priority
Dataset heterogeneity and limited scale	Partially addressed: Hosseini et al. (2025) multi-site CT (Iran + Iraq)	Impedes generalization to diverse populations	Multi-continental curation; federated deep learning	High
Class imbalance	Partially addressed: Wavelet equalization (Usman, 2025); balanced training (Jim, 2025)	Suppressed sensitivity for minority classes	Chaotic-optimized augmentation; cost-sensitive losses	Medium
Absence of external validation	Marginal: Hosseini multi-site; LCxNet on independent benchmark	Optimistic performance on single-site data	Prospective multi-site validation studies	High
Incomplete metric reporting	Persistent: multiple 2025-2026 studies omit SEN or SPEC	Prevents fair cross-study comparison	Adoption of TRIPOD reporting standards	High
MHA computational overhead	Addressed: XLLC-Net 99.62% at 60s/epoch; CL-PSO efficient	Limits deployment on limited-resource hardware	Combine lightweight CNN with MHA optimization	Medium
Absence of Global South validation	Not addressed: no African or South Asian clinical datasets	Unknown performance under different equipment and demographics	African and South Asian clinical dataset studies	Critical
No XAI-MHA integration	Not addressed; XAI present but separate from MHA objectives	Black-box models impede clinician trust and regulatory approval	Optimize jointly for accuracy and explanation fidelity	Critical
Lightweight MHA-CNN combination	Not addressed: lightweight and MHA-CNN studied separately across all 82 studies	Resource efficiency and optimized accuracy not achieved simultaneously	Integrate MHA-tuned hyperparameters into lightweight architectures	High

Note. TRIPOD = Transparent Reporting of a multivariable prediction model for Individual Prognosis Or Diagnosis; MHA = Metaheuristic Algorithm; XAI = Explainable Artificial Intelligence; CL-PSO = Comprehensive Learning PSO. Priority = Critical (field-defining), High (significant unmet need), or Medium (partially addressed).

Real-World Deployment Challenges: Regulatory, Bias, and Clinical Validation

The performance benchmarks documented in Tables 10, 11, and 12 were derived exclusively from controlled simulation environments or publicly available benchmark datasets, a context that systematically overstates the performance that clinical deployment would yield. Three categories of deployment challenge are identified from the reviewed literature.

Regulatory Considerations

No study in the 82-study corpus explicitly addresses the regulatory pathway required for clinical deployment of an MHA-optimized CNN. In the European Union, AI systems used for medical diagnosis are classified as high-risk under the EU Artificial Intelligence Act (2024), requiring conformity assessments, risk management documentation, and post-market monitoring, which are procedures that no reviewed MHA-CNN study has incorporated into its design. In the United States, FDA-cleared AI/ML-based software-as-medical-device

ISSN No. 2321-2705 | DOI: 10.51244/IJRSI |Volume XIII Issue IV April 2026

(SaMD) requires submission of algorithmic change protocols detailing how the model will be monitored and updated after deployment. MHA-optimized architectures, which update their hyperparameter configurations through iterative search, present specific challenges for such protocols because the model architecture itself is determined through an automated process that may not be reproducibly documented without explicit provenance tracking. Future work should integrate regulatory compliance as an explicit design constraint from the earliest stages of MHA-CNN framework development.

Dataset Bias and Domain Shift

The reviewed literature is dominated by studies using publicly available CT and histopathology datasets from North American, European, and East Asian populations, acquisition equipment, and imaging protocols. Domain shift, that is, the degradation of model performance when deployed on data from different populations or imaging equipment, represents a well-documented but systematically under-addressed risk in the field (Al-Salihi et al., 2026). Several studies report models achieving greater than 97% accuracy on held-out test sets drawn from the same dataset used for training, a result that provides limited evidence of generalizability. The meta-analytic standard deviations in Table 12 (CT unoptimized: SD=3.1%; CT hybrid MHA: SD=0.4%) suggest that MHA hybridization reduces within-modality performance variance; however, variance across sites and populations remains entirely undocumented for the majority of reviewed approaches. Federated learning frameworks, which train models across distributed datasets without centralizing patient data, represent a technically feasible and privacy-preserving mechanism for addressing both dataset bias and data access barriers in clinical settings (Prasad et al., 2024).

Clinical Validation and Integration

A fundamental distinction separates the diagnostic accuracy reported in computational studies from the clinical utility required for deployment as a decision support tool. Clinical utility requires demonstration that the AI system improves patient outcomes, reducing time to diagnosis, improving treatment selection, or reducing radiologist error rates, in prospective trials with appropriate comparator arms. None of the 82 reviewed studies reports prospective clinical trial data. The closest approximation is Ardila et al. (2019), who compared their end-to-end DL system against 11 radiologists on a shared dataset, establishing a form of reader study evidence. Future MHA-CNN frameworks should be designed with integration points for clinical workflow systems, including DICOM compatibility, SCADA/PACS integration, and clinician-facing interpretation interfaces, from the outset rather than as post-hoc additions. The XAI-integrated CNN frameworks emerging in 2025-2026 (Hussain et al., 2025; Jim et al., 2025) represent a necessary but not sufficient step toward this goal, providing interpretable outputs that can support clinician trust without yet establishing clinical outcome evidence.

CONCLUSION

This systematic review of 82 peer-reviewed studies published between 2019 and 2026 provides a comprehensive, cross-modality, meta-analytic synthesis of metaheuristic-optimized CNN frameworks for lung cancer detection. The evidence base supports three principal conclusions. MHA optimization consistently and substantially improves CNN classification performance. The meta-analytic data confirm a mean accuracy of 97.1% (SD=2.3%) for MHA-optimized approaches versus 93.6% (SD=3.1%) for unoptimized baselines across quantitatively reported CT studies, with hybrid MHA strategies extending the frontier to 99.5% (SD=0.4%). The sinusoidal chaotic map, identified as the best-performing chaotic variant across benchmarks, provides the theoretical foundation for STSOA-CNN's leading performance in the histopathology modality and its superior handling of minority class imbalance.

The 2025-2026 literature has introduced two significant advances not present in earlier work. First, Particle Swarm Optimization (PSO) hybridization with Bayesian surrogates, comprehensive learning strategies, and Flower Pollination dynamics has extended CT benchmark accuracy beyond 99.9% with reduced performance variance. Second, XAI integration through Grad-CAM and Saliency Maps has confirmed that CNN decision regions align with histologically recognized tissue markers, providing a necessary, though not sufficient, foundation for clinical deployment.

Three critical research gaps remain entirely unaddressed across all 82 included studies. The gaps are Global South clinical dataset validation, integration of XAI with MHA optimization objectives, and the combination of lightweight CNN design with MHA hyperparameter tuning. These gaps define the primary research frontier. A framework simultaneously addressing lightweight architecture, intrinsic XAI objectives, and regulatory-compliant design validated on African or Asian clinical datasets would represent the most consequential contribution available to the field and would advance clinical deployment accessibility, interpretability, and geographic equity in lung cancer detection.

REFERENCES

1. Abdulqader, A. F., Abdulameer, S., Bishoyi, A. K., Yadav, A., Kaur, G., Raghuvanshi, A., & Rao, K. (2025). Multi-objective deep learning for lung cancer detection in CT images: Enhancements in tumor classification, localization, and diagnostic efficiency. Discover Oncology, 16, Article 529. https://doi.org/10.1007/s12672-025-02314-8
2. Abhishek, G., Zuha, Z., Israr, A., & Zeeshan, A. (2022). A study on prediction of lung cancer using machine learning algorithms. International Journal of Computer Science and Technology, 106(15), 17–24.
3. Alam, T., Hsu, F. R., Hussain, T., & Rehman, A. (2025). A Comprehensive Review:Efficacy of Segmentation and Machine Learning, Deep Learning Techniques in Breast Tumor Detection. https://doi.org/10.36227/techrxiv.173609860.03508397/v1
4. Al-Salihi, N., Al-Masri, N., & Salih, M. (2026). Machine learning and deep learning in lung cancer diagnostics: A systematic review of technical breakthroughs, clinical barriers, and ethical imperatives. AI, 7(1), 23. https://doi.org/10.3390/ai7010023
5. Altuhaifa, F., & Albedah, A. (2025). FPA-based weighted average ensemble of deep learning models for classification of lung cancer using CT scan images. Scientific Reports, 15, 19024. https://doi.org/10.1038/s41598-025-02015-w
6. Ardila, D., Kiraly, A. P., Bharadwaj, S., Choi, B., Reicher, J. J., Peng, L., Tse, D., Etemadi, M., Ye, W., Corrado, G., Naidich, D. P., & Shetty, S. (2019). End-to-end lung cancer screening with three-dimensional deep learning on low-dose chest computed tomography. Nature Medicine, 25(6), 954–961. https://doi.org/10.1038/s41591-019-0447-x
7. Bhatia, S., Sinha, Y., & Goel, L. (2019). Lung cancer detection: A deep learning approach. In Soft Computing for Problem Solving (pp. 699–705). Springer. https://doi.org/10.1007/978-981-13-1735-1_66
8. Bijaya, K. H., & Thapa, H. C. (2020). Lung cancer detection using convolutional neural network on histopathological images. International Journal of Computer Trends and Technology, 68(10), 21–24. https://doi.org/10.14445/22312803/IJCTT-V68I10P104
9. Bingol, H., & Alatas, B. (2020). Chaos based optics inspired optimization algorithms as global solution search approach. Chaos, Solitons & Fractals, 141, Article 110434. https://doi.org/10.1016/j.chaos.2020.110434
10. Chintakayala, T., Nagabushanam, O., Priyadharshini, R., Palyam, R. J., & Radha, S. (2022). CNN architecture for lung cancer detection. Journal of Biomedical Informatics, 91, Article 103890.
11. Deepa, N., Prabadevi, B., Maddikunta, P. K., Gadekallu, T. R., Khan, M. A., Tariq, U., Reddy, T., & Baker, T. (2021). An AI-based intelligent system for healthcare analysis using Ridge-Adaline Stochastic Gradient Descent Classifier. The Journal of Supercomputing, 77(2), 1998–2017. https://doi.org/10.1007/s11227-020-03347-2
12. Dokeroglu, T., Sevinc, E., Kucukyilmaz, T., & Cosar, A. (2019). A survey on new generation metaheuristic algorithms. Computers & Industrial Engineering, 137, Article 106040. https://doi.org/10.1016/j.cie.2019.106040
13. European Union. (2024). The AI Act Explorer: EU Artificial Intelligence Act. Future of Life Institute. https://artificialintelligenceact.eu/ai-act-explorer/
14. Farghali, H., El-Sayed, A., Aboudi, M., & Ibrahim, S. (2025). Improving lung cancer detection with enhanced convolutional sequential networks. Scientific Reports, 15, Article 30482. https://doi.org/10.1038/s41598-025-06653-y

15. Fernandez-Castillo, E., Barbosa-Santillian, L., Falcon-Morales, L., & Sanchez-Escobar, J. (2022). Deep Splicer: A CNN model for splice site prediction in genetic sequences. Genes, 13(5), 907–1022. https://doi.org/10.3390/genes13050907
16. Hammad, M., ElAffendi, M., El-Latif, A. A. A., Ateya, A. A., Ali, G., & Plawiak, P. (2025). Explainable AI for lung cancer detection via a custom CNN on CT images. Scientific Reports, 15, 12707. https://doi.org/10.1038/s41598-025-97645-5
17. Hosseini, M. S., Raoofi, N., Boroujeni, S. R., Tabar, S. S., Vafaei, H., & Amini, S. (2025). Optimizing deep learning models for clinical lung cancer detection: Comparative analysis of segmentation-enhanced CNN-ensemble approaches in chest CT screening. International Journal of Computational Intelligence Systems, 18, 244. https://doi.org/10.1007/s44196-025-01069-y
18. Hussain, J., Ahmad, J., Ali, M., & Khan, A. (2025). LCxNet: An explainable CNN framework for lung cancer detection in CT images using multi-optimizer and visual interpretability. Applied Sciences, 8(5), 153. https://doi.org/10.3390/asi8050153
19. Islam, M. R., Rahman, M. M., Ali, M. S., Nafi, A. A. N., Alam, M. S., Godder, T. K., Miah, M. S., & Islam, M. K. (2024). Enhancing breast cancer segmentation and classification: An Ensemble Deep Convolutional Neural Network and U-net approach on ultrasound images. Machine Learning with Applications, 16, 100555. https://doi.org/10.1016/j.mlwa.2024.100555
20. Istiak, A., & Fahad, A. (2024). Early cancer detection using deep learning and medical imaging: A survey. Critical Reviews in Oncology/Hematology, 204, Article 104528. https://doi.org/10.1016/j.critrevonc.2024.104528
21. Jim, J. R., Rayed, M. E., Mridha, M., & Nur, K. (2025). XLLC-Net: A lightweight and explainable CNN for accurate lung cancer classification using histopathological images. PLOS ONE, 20(5). https://doi.org/10.1371/journal.pone.0322488
22. Kalaivani, N., Manimaran Sophia, S., & Devi, D. (2020). Deep learning based lung cancer detection and classification. International Journal of Advanced Computer Science and Applications, 8, 1–9.
23. Kasinathan, G., Jayakumar, S., Gandomi, A. H., Ramachandran, M., Fong, S. J., & Patan, R. (2019). Automated 3-D lung tumor detection and classification by an active contour model and CNN classifier. Expert Systems with Applications, 134, 112–119. https://doi.org/10.1016/j.eswa.2019.05.041
24. Kaur, J., Singh, P., & Arora, S. (2025). Lung cancer detection and classification using optimized CNN features and Squeeze-Inception-ResNeXt model. Computer Methods and Programs in Biomedicine, 265, Article 108428.
25. Lakshmanaprabu, S. K., Mohanty, S. N., Shankar, K., Arunkumar, N., & Ramirez, G. (2019). Optimal deep learning model for classification of lung cancer on CT images. Future Generation Computer Systems, 92, 374–382. https://doi.org/10.1016/j.future.2018.10.009
26. LeCun, Y., Bengio, Y., & Hinton, G. (2015). Deep learning. Nature, 521(7553), 436–444. https://doi.org/10.1038/nature14539
27. Litjens, G., Kooi, T., Bejnordi, B. E., Setio, A. A. A., Ciompi, F., Ghafoorian, M., Van Der Laak, J. A. W. M., Van Ginneken, B., & Sánchez, C. I. (2017). A survey on deep learning in medical image analysis. Medical Image Analysis, 42, 60–88. https://doi.org/10.1016/j.media.2017.07.005
28. Liu, C., Hu, S. C., Wang, C., Lafata, K., & Yin, F. F. (2020). Automatic detection of pulmonary nodules on CT images with YOLOv3: Development and evaluation using simulated and patient data. Quantitative Imaging in Medicine and Surgery, 10(10), 1917–1929. https://doi.org/10.21037/qims-19-883
29. Mathivanan, S. K., Subramanian, K., Saravanan, V., Jayagopal, P., & Kumar, N. (2025). Enhanced superpixel-guided ResNet framework with optimized deep-weighted averaging-based feature fusion for lung cancer detection in histopathological images. Diagnostics, 15(7), 805. https://doi.org/10.3390/diagnostics15070805
30. Mehdi, S., Chauhan, A., & Dhutty, A. (2023). Cancer and new prospective to treat cancer. International Journal of Current Pharmaceutical Research, 15(6), 16–22.
31. Mirrashid, M., & Naderpour, H. (2021). Transit search: An optimization algorithm based on exoplanet exploration. Results in Engineering, 12, Article 100284. https://doi.org/10.1016/j.rineng.2021.100284
32. Narmada, K., Prabakaran, G., & Mohan, S. (2019). Classification and stage prediction of lung cancer using convolutional neural networks. International Journal of Innovative Technology and Exploring Engineering, 8(10), 993–998.

33. Nithila, E. E., & Kumar, S. S. (2019). Segmentation of lung from CT using various active contour models. Biomedical Signal Processing and Control, 47, 57–62. https://doi.org/10.1016/j.bspc.2018.08.008
34. Omprakash, K., & Samiappan, D. (2025). A novel two-stage deep learning approach for lung cancer using enhanced ResNet50 segmentation and LungSwarmNet classification. Scientific Reports, 15, 41889. https://doi.org/10.1038/s41598-025-31000-6
35. Page, M. J., McKenzie, J. E., Bossuyt, P. M., Boutron, I., Hoffmann, T. C., Mulrow, C. D., Shamseer, L., Tetzlaff, J. M., Akl, E. A., Brennan, S. E., Chou, R., Glanville, J., Grimshaw, J. M., Hróbjartsson, A., Lalu, M. M., Li, T., Loder, E. W., Mayo-Wilson, E., McDonald, S., … Moher, D. (2021). The PRISMA 2020 statement: An updated guideline for reporting systematic reviews. BMJ, n71. https://doi.org/10.1136/bmj.n71
36. Ponnada, V. T., & Srinivasu, S. V. N. (2019). Efficient CNN for lung cancer detection. International Journal of Recent Technology and Engineering, 8(2), 3499–3503.
37. Prasad, U., Chakravarty, S., & Mahto, G. (2024). Lung cancer detection and classification using deep neural network based on hybrid metaheuristic algorithm. Soft Computing, 28, 8579–8602. https://doi.org/10.1007/s00500-023-08845-y
38. Raghuvanshi, S. S., Arya, K. V., & Patel, V. (2024). PSbBO-Net: A hybrid particle swarm and Bayesian optimization-based DenseNet for lung cancer detection using histopathological and CT images. International Journal of Electrical and Electronics Research, 12(3), 1074–1086.
39. Roy, K., Chaudhury, S. S., Burman, M., Ganguly, A., Dutta, C., Banik, S., & Banik, R. (2019). A Comparative study of Lung Cancer detection using supervised neural network. 2019 International Conference on Opto-Electronics and Applied Optics (Optronix), 1–5. https://doi.org/10.1109/OPTRONIX.2019.8862326
40. Sabri, M., Al-Dhlan, K. A., & Alrashidi, M. (2025). Enriched lung cancer classification approach using an optimized hybrid deep learning approach. Scientific Reports, 15, Article 37573. https://doi.org/10.1038/s41598-025-07322-w
41. Shailesh, K. T., Dhirendra, P. S., & Jaytrilok, C. (2020). Lung cancer identification: A review on detection and classification. Cancer and Metastasis Reviews, 39(4), 989–998. https://doi.org/10.1007/s10555-020-09901-x
42. Shan, W., Qiao, Z., Heidari, A. A., Chen, H., Turabieh, H., & Teng, Y. (2021). Double adaptive weights for stabilization of moth flame optimizer: Balance analysis, engineering cases, and medical diagnosis. Knowledge-Based Systems, 214, Article 106728. https://doi.org/10.1016/j.knosys.2020.106728
43. Sharma, K. R., Goyal, B., Gupta, M., Sharma, T., & Dogra, A. (2023). Breast Cancer Detection Methodologies using Image Processing: Current Trends and Era in Machine Learning and Risk Mitigation. Open Neuroimaging Journal, 16. https://doi.org/10.2174/18744400-v16-e230704-2022-2
44. Shukla, R., Garg, A., & Misra, P. (2025). Transfer learning based deep architecture for lung cancer classification using CT image with pattern and entropy based feature set. Scientific Reports, 15, 27156. https://doi.org/10.1038/s41598-025-13755-0
45. Siegel, R. L., Miller, K. D., Fuchs, H. E., & Jemal, A. (2023). Cancer statistics, 2023. CA: A Cancer Journal for Clinicians, 73(1), 7–33. https://doi.org/10.3322/caac.21763
46. Sujatha, R., Krishnan, S., Chatterjee, J. M., & Gandomi, A. H. (2025). Advancing plant leaf disease detection integrating machine learning and deep learning. Scientific Reports, 15(1), 11552. https://doi.org/10.1038/s41598-024-72197-2
47. Sung, H., Ferlay, J., Siegel, R. L., Laversanne, M., Soerjomataram, I., Jemal, A., & Bray, F. (2021). Global cancer statistics 2020: GLOBOCAN estimates of incidence and mortality worldwide for 36 cancers in 185 countries. CA: A Cancer Journal for Clinicians, 71(3), 209–249. https://doi.org/10.3322/caac.21660
48. Tsimenidis, S., Vrochidou, E., & Papacostas, G. (2022). Omics data and data representation for deep learning based predictive modelling. International Journal of Molecular Sciences, 23(12), 272–296. https://doi.org/10.3390/ijms23126294
49. Usman, M., Hussain, A., & Zhang, Z. (2025). A novel ensemble transfer learning approach for lung cancer classification using advanced VGGNet16 with wavelet transform equalization and CL-PSO.

Computers in Biology and Medicine, 191, Article 109952. https://doi.org/10.1016/j.compbiomed.2025.109952

50. Wang, Y., Gao, S., Yu, Y., Cai, Z., & Wang, Z. (2021). A gravitational search algorithm with hierarchy and distributed framework. Knowledge-Based Systems, 218, Article 106877. https://doi.org/10.1016/j.knosys.2021.106877
51. World Health Organization [WHO]. (2023). Lung cancer [WHO]. World Health Organization. https://www.who.int/news-room/fact-sheets/detail/lung-cancer
52. Xie, L., Han, T., Zhou, H., Wang, D., Tan, D., & Liu, L. (2021). Tuna swarm optimization: A novel swarm-based metaheuristic algorithm for global optimization. Computational Intelligence and Neuroscience. https://doi.org/10.1155/2021/9210050
53. Xing, Y. X., Wang, J. S., Zhang, S. W., Zhang, S. H., Ma, X. R., & Zhang, Y. H. (2024). Transit search algorithm based on oscillation exploitation factor and Roche limit for wireless sensor network deployment optimization. Artificial Intelligence Review, 58, Article 29. https://doi.org/10.1007/s10462-024-10986-3
54. Xu, Z., Yang, H., Li, J., Zhang, X., Lu, B., & Gao, S. (2021). Comparative study on single and multiple chaotic maps incorporated grey wolf optimization algorithms. IEEE Access, 9, 42654–42672. https://doi.org/10.1109/ACCESS.2021.3083220
55. Yamashita, R., Nishio, M., Do, R. K., & Togashi, K. (2018). Convolutional neural networks: An overview and application in radiology. Insights into Imaging, 9(4), 611–629. https://doi.org/10.1007/s13244-018-0639-9
56. Yang, X. S. (2020). Nature-inspired optimization algorithms: Challenges and open problems. Journal of Computational Science, 46, Article 101104. https://doi.org/10.1016/j.jocs.2020.101104
57. Zamanidoost, Y., Ould-Bachir, T., & Martel, S. (2025). OMS-CNN: Optimized multi-scale CNN for lung nodule detection based on faster R-CNN. IEEE Journal of Biomedical and Health Informatics, 29(3), 2148–2160. https://doi.org/10.1109/JBHI.2024.3507360
58. Zhao, D., Liu, L., Yu, F., Heidari, A. A., Wang, M., Liang, G., Muhammad, K., & Chen, H. (2021). Chaotic random spare ant colony optimization for multi-threshold image segmentation of 2D Kapur entropy. Knowledge-Based Systems, 216, Article 106510. https://doi.org/10.1016/j.knosys.2020.106510
59. Zia, U., Yan, Q., Long, W., Yiwei, S., Qianqian, Y., Saeed, U. K., Rukhma, A., & Juanjuan, Z. (2024). Effective lung nodule detection using deep CNN with dual attention mechanisms. Journal of Computational Science, 81, Article 102368. https://doi.org/10.1016/j.jocs.2024.102368